Energetics and Crystal Chemical Systematics among Ilmenite, Lithium Niobate, and Perovskite Structures

Alexandra Navrotsky

Thermochemistry Facility, Chemistry Annex, Department of Chemical Engineering and Materials Science, University of California at Davis, One Shields Avenue, Davis, California 95616

Received March 25, 1998. Revised Manuscript Received June 5, 1998

Transitions from chain silicates to garnet, ilmenite, and perovskite structures are important in deep earth geophysics and solid-state chemistry. Titanates and other oxides also show polymorphism among ilmenite, lithium niobate (metastable), and perovskite structures. This review brings together the evidence from the recent mineralogical and materials science literature linking the crystal chemistry, thermodynamics, and occurrence of these polymorphs at high pressure and temperature. A-site ordered multicomponent titanate perovskites are also discussed. A common feature of the perovskite structure is its high vibrational entropy.

Contents

Introduction

Pressure and temperature-induced phase transitions in ABO_3 oxides (A = transition metal or alkaline earth; B = Si, Ge, Ti) are important in earth science, materials science, and fundamental solid-state chemistry. The geologic interest arises from the likely existence of a phase approaching $MgSiO_3$ in composition and having the perovskite structure as a major component of the Earth's lower mantle.[1,2] In addition both $CaTiO_3$ perovskite and $FeTiO_3$ ilmenite are important accessory minerals and provide constraints on thermodynamic parameters such as oxygen fugacity and silica activity in igneous systems.[3] The significance for materials science comes from the structure−property relations of these different structure types. The search for better ferroelectric and nonlinear optical materials pinpoints the lithium niobate structure,[4] while the perovskites, with various cation ordering schemes, vacancy compensation, and distortional transitions, offer a wealth of ceramic, dielectric, and optical materials.[5] From the point of view of solid-state chemistry, the fundamental question is which structure forms under what conditions of pressure, temperature, and bulk composition.[6] The relation of thermodynamics and crystal chemistry is the link between macroscopic (ΔH, ΔS, ΔV) and microscopic (bond lengths, tolerance factors, lattice vibrations, electronic structure) properties in these materials. This review summarizes these fundamental relations for silicates, germanates, titanates, and other related materials.

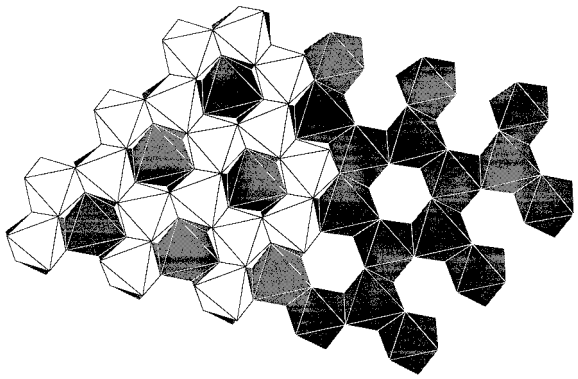

Figure 1. Ilmenite (ABX_3) structure projected on (001). The layers of octahedra occupied by A (shaded) and B (white) alternate. In the corundum structure, A and B are identical.

Description of Structures, Taken Closely from Navrotsky[1]

When both cations in ABO_3 are similar in size and occupy octahedral sites, structures based on ordered derivatives of the corundum structure are formed. The basic structure (see Figures 1 and 2) contains almost hexagonal close packed oxygen layers with cations defining octahedral layers perpendicular to the *c*-axis. The occupancy of each layer (see Figure 2a) is identical in the corundum structure (Al_2O_3, Fe_2O_3, and Cr_2O_3), and each octahedron is slightly distorted as shown by the *c*/*a* ratio. When two different ions form a ternary ABO_3 structure such as that of ilmenite, $FeTiO_3$, they order in alternate layers (see Figure 2b). The iron and titanium octahedra then have different metal−oxygen

10.1021/cm9801901 CCC: $15.00
Published on Web 08/29/1998

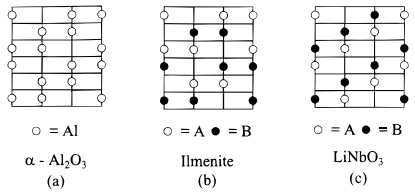

Figure 2. Representation of sesquioxide structures showing (a) the disordered (corundum) and the two ordered subfamilies of structures: (b) ilmenite and (c) lithium niobate. The horizontal lines represent the close-packed oxygen planes. The cations occupy the octahedral holes. After Mehta and Navrotsky.[4]

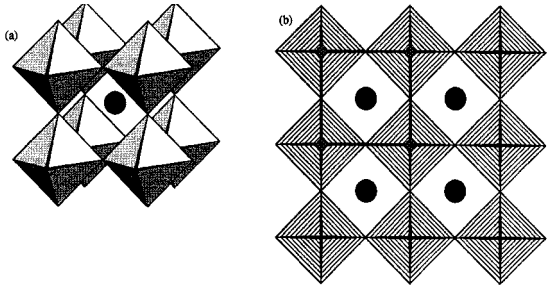

Figure 3. Representation of the ideal cubic perovskite structure. Left (a) shows coordination polyhedra; right (b) shows linkage of octahedra. Spheres represent "A" site cations. "B" site cations reside at center of octahedra.

bond lengths and different degrees of distortion. The ordered structure is a superstructure of the basic corundum type, and the space group of ilmenite ($R\bar{3}$) is a subgroup of that of corundum ($R\bar{3}2/c$). In a solid solution series such as hematite−ilmenite, Fe_2O_3−$FeTiO_3$, order can appear gradually as a higher order phase transition.[7]

A different pattern of occupancy of octahedral sites in a hexagonal oxygen array is encountered in the lithium niobate structure, exemplified by $LiNbO_3$ (see Figure 2c). The octahedral sites occupied are the same ones as in corundum or ilmenite. However, instead of unlike ions segregating into alternate layers as in ilmenite, each layer in the lithium niobate structure contains both species in equal proportions, ordered such that each cation shares three octahedral edges with one of the opposite type. In this way no cation is bridged through two oxygens to another like cation. The lithium niobate structure can also be described as a very distorted derivative of the perovskite type, to which it can be related by a displacive transformation.

When the A cation requires much longer bond lengths and a higher coordination number than the B cation, the perovskite structure, named after a mineral of idealized composition, $CaTiO_3$, can form. It consists of a framework of virtually regular BO_6 octahedra linked through all their corners (see Figure 3). If the octahedra form an ideal cubic array, the interstices between them define a site, surrounded by 12 equidistant anions, that is occupied by the large A cation. Because the octahedra form an interconnected framework, one can change the bond length in the central site only by perturbing the octahedra. The most common perturbations involve tilting or puckering of the octahedral framework. This distortion leaves the octahedra regular in shape but brings some oxygens closer to the cation in the central site, decreasing its coordination number from 12 to 10, 8, or even smaller. Several different distortions are commonly seen.[8] These distortions allow a much wider range of cation sizes to be accommodated in the perovskite structure than the ideal cubic arrangement would permit. One can define a tolerance factor, t, for a perovskite ABO_3 as

$$t = \frac{r_{AO}}{2^{1/2} r_{BO}} = \frac{r_A + r_O}{2^{1/2}(r_B + r_O)} \quad (1)$$

where the r terms are bond lengths calculated as sums of ionic radii. If $t = 1$, then both cations can be accommodated in the ideal cubic perovskite with their optimum cation−anion bond lengths. If t deviates from unity, typically in the range 0.8−1.1, a perovskite may still form, with the degree of distortion from cubic symmetry increasing and the thermodynamic stability decreasing with increasing values of the absolute value of $(1 - t)$.[9] The type and extent of distortion depend sensitively on temperature, pressure, and composition.[10−14]

Phase Transitions, the Ionic Model, and Thermodynamic Driving Forces

In these systems, as the size of the tetravalent cation increases (Si, Ge, Ti), phases encountered only at very high pressure for smaller tetravalent cations occur at lower pressures or atmospheric pressure for larger cations. Thus the germanates and titanates have long been considered as more readily accessible analogues for high-pressure silicates. Detailed structural and thermodynamic study, however, shows that the systematics relating bond lengths to stability are complex in that the effects of energy (ΔE or ΔH), entropy ($T\Delta S$), and volume ($\int \Delta V dP$) are of comparable magnitude and must be considered together in determining the $P-T$ stability field of a given structure. In addition to a considerable body of work on silicate and germanate phase transitions in the past 15 years, the titanates have sparked renewed interest because they show several new high-pressure structures.

The geochemical community has generally viewed these materials from the point of view of simple ionic models. The thermochemical data summarized here suggest that such models, using ionic radius, or metal−oxygen bond length, as a correlating parameter, work surprisingly well. Perhaps this is in part because the optimized sets of radii de facto include the effects of covalency, crystal field, and other bonding factors. The general success of parametrized interatomic potentials for structure, energy, and lattice dynamical simulations (see below) probably reflects the same regularity of optimized cation−oxygen distances. In any case, the thermochemical data summarized below appear to confirm the adequacy of a basically ionic approach to structural transitions in ABO_3 compounds.

Phase Transitions in Silicates and Germanates

At atmospheric pressure the $ASiO_3$ and $AGeO_3$ (A = alkaline earth of divalent transition metal) phases crystallize as chain structures (pyroxenes or pyroxenoids), which contain linked silicate or germanate tetrahedra separated by divalent cations in distorted 6-

Table 1. Thermochemical Parameters for High-Pressure Phase Transitions in Silicates and Germanates

	transformation				
	P (GPa)	T (°C)	$\Delta H°$ (kJ/mol)	$\Delta S°$ (J/K·mol)	$\Delta V°$ (cm^3/mol)
pyroxene or pyroxenoid = garnet					
$CaGeO_3$[15]	1	1000	−4.90	−5.9	−5.97
$CdGeO_3$[61]	1	1000	+0.6	−8.4	−5.30
$MnSiO_3$[62]	12	1000	+34.6	−6.7	−4.00
$MgSiO_3$[40]	16	1800	35.1	−2.0	−2.83
pyroxene = ilmenite					
$MgGeO_3$[64]	6	1200	7.5	−6.3	−5.11
$MgSiO_3$[39]	metastable		59.0	−15.5	−4.94
$ZnSiO_3$[63,65]	10.5	1000	52.0	−14.3	−6.36
garnet = perovskite					
$CaGeO_3$[15]	10	1000	+43.3	+10.9	−5.35
$CdGeO_3$[61]	metastable		+43.1	−1.7	−4.88
$MgSiO_3$[37,38,40]	22	2000	75.0	−7.5	
ilmenite = perovskite					
$MgSiO_3$[37,38]	24	1300	43.2	3.6	−1.91
$CdGeO_3$[61]	10	1000	34.3	4.6	−3.09
other					
$CaSiO_3$[a] 66	12	1400			
$ZnGeO_3$[b] 65	3.5	900			
$CdGeO_3$[d] 61	7	1000	8.8	−1.3	−1.76
$SrGeO_3$[c] 67	6	1000			

[a] $^1/_3CaSi_2O_5 + {}^1/_3Ca_2SiO_4 \rightarrow CaSiO_3$ (perovskite). [b] $^1/_2Zn_2GeO_4$ (tetrag. spinel) + $^1/_2$ GeO_2 (rutile) → $ZnGeO_3$ (ilmenite). [c] $SrGeO_3$ (pyroxenoid → perovskite). [d] $CdGeO_3$ (garnet → ilmenite).

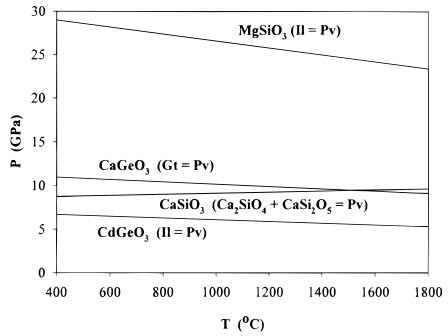

Figure 4. $P-T$ slopes for perovskite-forming reactions in silicates and germanates. References in Table 1.

or 8-fold coordination. As pressure increases, new structures form, including garnet, ilmenite, and perovskite. Table 1 summarizes the occurrence and energetics of these phases. The coordination number of Si or Ge increases from 4 in the chain silicates, to a mixture of 4 and 6 in garnet, to 6 in ilmenite and perovskite. The coordination of the divalent cation is mainly distorted 6-fold in chain silicates, a mixture of 6-fold and 8-fold in garnet, regular octahedral in ilmenite, and distorted 8-fold in perovskite. In general, while volume decreases in the sequence pyroxene, garnet, ilmenite, perovskite, entropy decreases in the series pyroxene, garnet ∼ perovskite, ilmenite[13] (see Table 1). Thus the perovskite is a high-entropy phase with a negative $P-T$ slope for its formation (see Figure 4); since, by the Clausius−Clapeyron equation, $dP/dT = \Delta S/\Delta V$.

The source of these irregular entropy−volume relations lies in the changing vibrational density of states. Replacing tetrahedral Si or Ge with octahedral Si or Ge increases the Si−O or Ge−O bond length and weakens the bond, displacing its stretching vibration to much lower frequency. A number of vibrational density of states models have been used to compute the heat capacity and entropy of these phases.[1,14−20] Though they differ in detail, all these models predict a higher vibrational entropy for the perovskite than for the ilmenite phase. This entropy difference is most pronounced for the smallest A-site cations (e.g., Mg).

The question of distortional phase transitions in silicate perovskites is important to the elasticity and equation of state of minerals and, thus, to interpreting seismic data. A number of theoretical calculations have been applied to the lattice dynamics and stability of $CaSiO_3$[14,21] and $MgSiO_3$[14,19−21] perovskites, as well as for titanate perovskites.[22,23] Though some calculations[20,24] suggest the possibility of orthorhombic to tetragonal to cubic transitions in $MgSiO_3$ perovskite, other calculations,[21,25] generally using more refined theory, conclude that the cubic phase of $MgSiO_3$ is too high in energy relative to the orthorhombic to be attained at any temperature below the melting point. Earlier experimental studies on quenched $MgSiO_3$ perovskite hinted at the possibility of a cubic high-temperature phase.[26,27] More recent structural studies, now possible within the high $P-T$ stability field of $MgSiO_3$ perovskite,[28] suggest that, although slight changes in c/a ratio occur as a function of P and T, the phase remains orthorhombic up to 1700 °C and 36 GPa, that is, throughout much of the lower mantle.

$CaSiO_3$ perovskite is interesting in that, although it is stable at lower pressure (12 GPa) than $MgSiO_3$ perovskite (>22 GPa), it is not quenchable to ambient conditions, transforming, below about 3 GPa, to an amorphous phase.[29−31] Recent calculations[32,33] have identified Brillouin zone edge dynamical instabilities in the cubic perovskite. The coupling of the low-frequency ferroic mode with octahedral tilting modes and strain may lower the activation energy for amorphization.[33]

The $P-T$ phase diagram for $MgSiO_3$ composition[34] is shown in Figure 5. Competition between a number of assemblages rather closely balanced in thermodynamic properties causes considerable complexity at 10−20 GPa. However, it is clear that the perovskite phase dominates above 24 GPa. Garnet is a high-temperature phase, probably stabilized by Mg−Si disorder on octahedral sites.

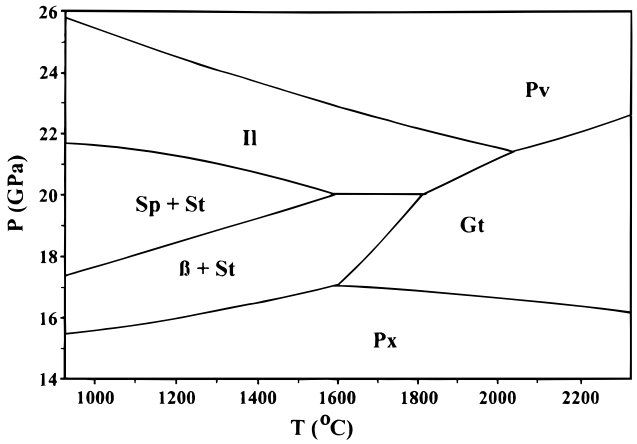

Figure 5. $MgSiO_3$ phase diagram simplified from Akaogi.[34] Px = pyroxene, β = wadsleyite, a spinelloid, Sp = spinel, St = stishovite, the rutile form of SiO_2, Il = ilmenite, Pv = perovskite, Gt = garnet.

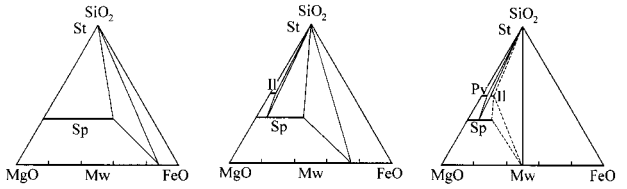

Figure 6. MgO−FeO−SiO_2 phase relations at 1100 °C and pressures between 19 and 26 GPa. St = stishovite, Mw = magnesiowustite, Sp = spinel, Pv = perovskite. Figure modified from ref 69.

Figures 6 and 7 show the behavior of the MgO−FeO−SiO_2 system at pressures above 20 GPa.[35,36] The field of perovskite is limited to Mg-rich compositions and terminated by a phase field containing a rocksalt (Fe,Mg)O (magnesiowustite) solid solution and SiO_2 stishovite having the octahedrally coordinated rutile structure. These relations are probably complicated by the presence of substantial ferric iron in the perovskite phase and its consequent defect equilibria[53] but details are still sparse. The ilmenite (Fe,Mg)SiO_3 phase also exists only at low iron content, but its stability has not been investigated in detail.

Phase Transitions in Titanates and Related Systems

$MgTiO_3$ and the transition metal titanates crystallize in the ilmenite structure at 1 atm. $CdTiO_3$[41] and $CdSnO_3$[42] are dimorphic; the ilmenite phase is the low-temperature polymorph, the perovskite the high temperature form. The transition requires hydrothermal conditions to aid kinetics, but a phase transition at 1 atm is clearly indicated (see Figure 8). The perovskite phase is denser than the ilmenite. As the high temperature form, it has the higher entropy, and the $P-T$ slope for the transition is negative, indeed more strongly negative than for the silicates and germanates.

$MnTiO_3$[43−46,51] and $FeTiO_3$[44,47−50] ilmenites transform to high-pressure polymorphs (see Figure 8). Initially indexed as having disordered ilmenite (corundum) structures,[44] the materials quenched from high pressure and high-temperature studies were later shown to have the lithium niobate structure.[45,47] When these lithium

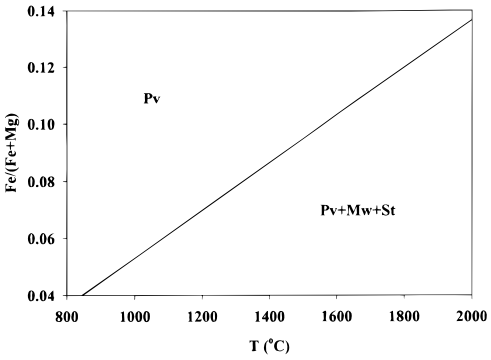

Figure 7. Solubility limit (best fit line to synthesis data) of iron (Fe/(Fe + Mg)) in $Fe_xMg_{1-x}SiO_3$ perovskite at 26 GPa as a function of temperature. Simplified from ref 35. Pv = perovskite, Mw = magnesiowustite, St = stishovite.

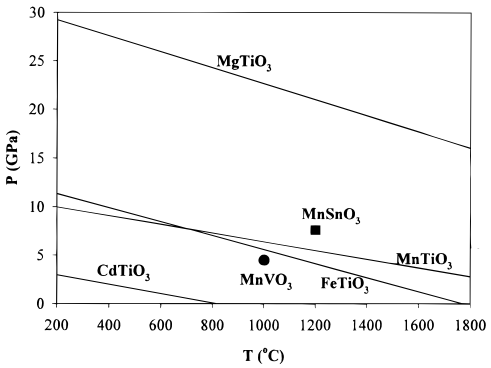

Figure 8. Ilmenite−perovskite phase transitions in titanates and related compounds. Lines represent measured $P-T$ boundaries; points represent single (P, T) points of transition. References in Table 2.

niobate materials were compressed at room temperature in a diamond anvil cell,[46,48] they transformed to a perovskite structure at pressures far lower than the ilmenite−lithium niobate transition seen in multianvil quench experiments. This perovskite phase reverted to the lithium niobate on pressure release. It is now generally accepted that the perovskite is the stable structure at high P and T, and the lithium niobate forms by a diffusionless transition on pressure release and is a metastable quench product.[46,48−50] Similar transitions were recently seen in $MgTiO_3$, but at higher pressures than for $MnTiO_3$ or $FeTiO_3$.[49,50] Again, the lithium niobate phase appears to be a quench product of the perovskite.

Intermediate compositions along the $FeTiO_3-MgTiO_3$ join also transform to a high pressure phase, which, though probably a perovskite in situ at high P and T, is recovered as a lithium niobate solid solution.[49,50] This is the first documentation of complete and continuous substitution of Mg^{2+} by Fe^{2+} in the perovskite A site.

Calorimetric studies have measured the enthalpy difference between ilmenite and perovskite in $CdTiO_3$[9,52] and between ilmenite and lithium niobate quench phase in $MnTiO_3$,[51] $FeTiO_3$,[47,50] $MgTiO_3$,[50] and $MgTiO_3-FeTiO_3$ solid solutions.[50] Thermodynamic data are summarized in Table 2. There is a linear increase in the $\Delta H°$ of transition between lithium niobate and ilmenite with increasing Mg content in $FeTiO_3-MgTiO_3$.[50] Similarly, $\Delta H°$ (ilmenite = lithium niobate) is a linear function of "A" cation size for a variety of

Table 2. Thermodynamic Properties of High-Pressure $MTiO_3$ Phases and Related Compounds

	transition observed		thermodynamic properties		
	P (GPa)	*T* (°C)	$\Delta H°$ (kJ/mol)	$\Delta S°$ (J/K·mol)	$\Delta V°$ (cm^3/mol)
ilmenite = perovskite					
$MgTiO_3$[49,50]	21	1200	33.1	5.5	−1.56
$MnTiO_3$[46,51]	6.7	1200	21.3	7.9	−1.76
$FeTiO_3$[49,50]	11	1200	27.1	8.9	−1.55
$CdTiO_3$[41,52]	0.001	830	15.0	14.2	−1.78
$MnVO_3$[68]	4.5	1200			−2.10
$NaNbO_3$[4]	ilmenite metastable		−5.5		
ilmenite = lithium niobate					
$MgTiO_3$[49,50]			28.8	4.0	−0.16
$MnTiO_3$[51]			8.4	(−24.2)	−0.44
$FeTiO_3$[47,49,50]			14.5	4.9	−0.30
$LiNbO_3$[4]	ilmenite metastable		−9.8		
lithium niobate = perovskite (metastable)					
$MgTiO_3$[50]	22−28	25	4.4	1.5	−1.40
$MnTiO_3$[46,51]	2.5	25	12.9	32.1	−1.32
$FeTiO_3$[50]	16	25	12.3	4.0	−1.25
$MnSnO_3$[48]	7.5	25			

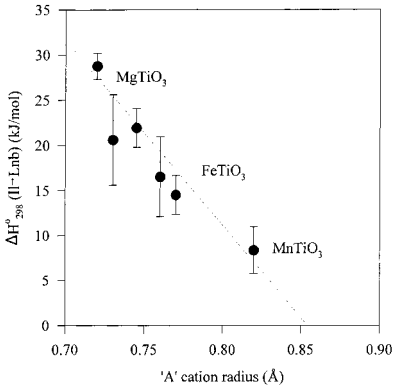

Figure 9. Enthalpy difference between lithium niobate (quench phase) and ilmenite structure versus A cation radius. ΔH from calorimetric data; see Table 2. Points between $MgTiO_3$ and $FeTiO_3$ represent $Mg_{1-x}Fe_xTiO_3$ solid solutions.[58]

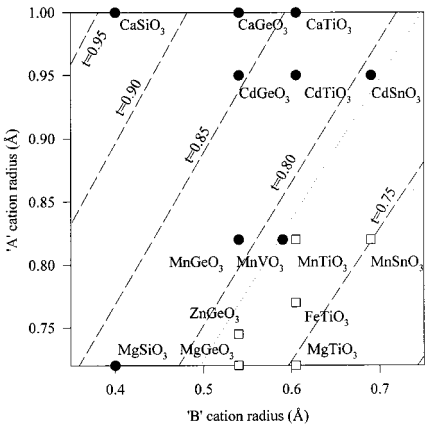

Figure 10. Goldschmidt diagram showing occurrence of perovskite and lithium niobate phases as function of A and B cation radii.[50] Solid circles represent systems where a lithium niobate phase is not observed; open squares represent systems with a lithium niobate quench phase.

titanates[50] (see Figure 9). This suggests that Fe is not acting differently from Mg due to specific electronic effects; rather the size of the A cation dominates in the energetics.

Different perovskite forming oxides of the type $A^{2+}B^{4+}O_3$ are compared in Figure 10 by using a Goldschmidt diagram, which plots the "B" cation radius versus the A cation radius for 6-fold coordination.[50] Lines of equal value of tolerance factor are indicated.

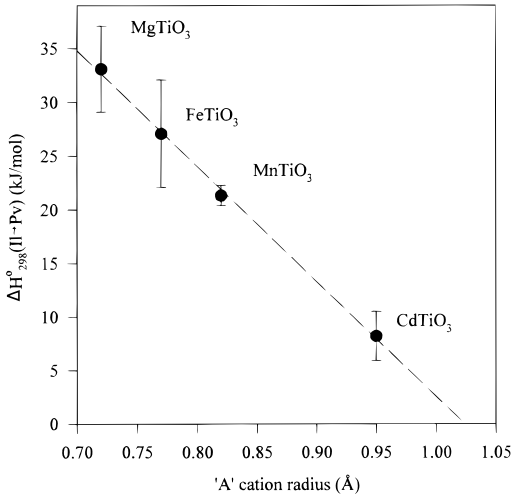

Figure 11. Enthalpy of ilmenite−perovskite transition in titanates vs A cation radius.[50] ΔH calculated from $P-T$ boundaries. References from Table 2.

Figure 11 shows the enthalpy (calculated from the $P-T$ diagram) for the ilmenite−perovskite transition versus the A-cation radius.[50] The data define a straight line with the $\Delta H°_{298} = 0$ intercept at 1.02 ± 0.04 Å. The radius of Ca is 1.00 Å, and $CaTiO_3$ is stable as a perovskite at ambient conditions. There is thus a clear relationship between A cation size and the energetic cost of forming a perovskite.

The Goldschmidt diagram (Figure 10) suggests that the lithium niobate quench phase occurs only for tolerance factors less than about 0.78 or, in titanates, for divalent cation radii less than about 0.8 Å. The trends predict that $CoTiO_3$ and $NiTiO_3$ ilmenites could form high-pressure perovskite structures which would quench to lithium niobate phases. The best chance for finding these phases would be at high temperature (1400−1800 °C) because the competing decomposition to oxides (AO (rocksalt) + TiO_2 (rutile or high-pressure phase)) would have a positive dP/dT, while the ilmenite−perovskite transition would have a negative dP/dT. Decomposition of $ATiO_3$ ilmenites (A = Mg, Ni, Co, Zn) to binary oxide mixtures was noted by Ito and Matsui.[60] In view of the recent discovery of $MgTiO_3$ perovskite and lithium niobate phases,[49,50] these other systems merit a closer look with modern high $P-T$ techniques.

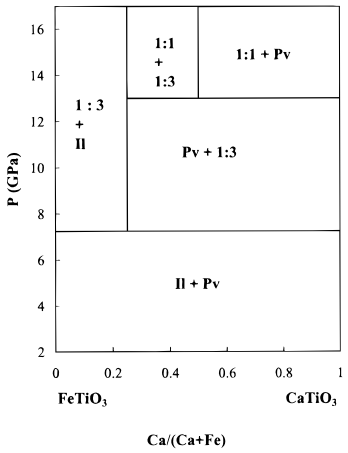

Figure 12. Phase boundaries for formation of ordered (Ca,Fe)TiO_3 perovskites at 1200 °C.[58] Il = ilmenite, Pv = perovskite, 1:3 = $Fe_3CaTi_4O_{12}$, 1:1 = $FeCaTi_2O_6$.

The trends clearly show that $MgSiO_3$ perovskite should not form a lithium niobate on quenching. This perovskite is indeed retained on pressure release.[34] Similarly, $CaSiO_3$ perovskite, on quenching, rather than forming a lithium niobate, has an instability leading to amorphization.[33]

High-pressure phase transitions involving ilmenite, lithium niobate, and perovskite phases in some other related materials are also included in Table 2.

The $FeTiO_3$–$CaTiO_3$ System

At 1 atm, the join $FeTiO_3$–$CaTiO_3$ exhibits no intermediate compounds and almost no solid solution (<2 mol % solubility) between $FeTiO_3$ (ilmenite) and $CaTiO_3$ (perovskite).[54] At high pressure (see Figure 12) there is still almost no solid solution, but two intermediate ordered perovskite phases, $CaFeTi_2O_6$ and $CaFe_3Ti_4O_{12}$, exist.[55,56] The $CaFe_3Ti_4O_{12}$ or 1:3 phase has a cubic double perovskite structure with the *Im*3 space group,[55] while the $CaFeTi_2O_6$ or 1:1 phase has a tetragonal double perovskite structure with the space group $P4_2/nmc$.[56,57] In both these compounds, Ca^{2+} and Fe^{2+} are ordered in different A-site positions. In $CaFe_3Ti_4O_{12}$ all Fe^{2+} is in approximately square planar coordination, while in $CaFeTi_2O_6$ the Fe^{2+} occupies two sites, one with square planar coordination and the other with tetrahedral coordination.

It is notable that the ordered phases form at pressures below the formation of $FeTiO_3$ perovskite and before any significant structural changes in $CaTiO_3$. A recent phase equilibrium and thermochemical study[51] confirms the stability of these ordered phases and allows calculation of phase relations (see Table 3). Both ordered perovskites form along negative $P-T$ boundaries, showing that, even though they have no cation disorder, they are of higher vibrational entropy than corresponding mixtures of $FeTiO_3$ (ilmenite) and $CaTiO_3$ (perovskite). Phase relations in $FeTiO_3$–$CaTiO_3$ at 1200 °C, calculated from thermochemical data, are shown in Figure 13. An invariant point for the coexistence of the 1:1 phase, the 1:3 phase, $CaTiO_3$ (perovskite), and $FeTiO_3$ (ilmenite) is 1518 °C and 5.3 GPa.

The volume change in forming the phase 1:3 is greater in magnitude than for forming 1:1, but the entropy and enthalpy forming the 1:1 phase are slightly larger (based on a common number of oxygens, i.e., $Ca_xFe_{1-x}TiO_3$). Thus these ordered perovskites are favored by both high pressure (negative ΔV) and high temperature (positive ΔS).

Table 3. Thermochemical Data for Reactions Involving (Fe,Ca)TiO_3 Phases[58]

reaction[a]	$\Delta V°_{298}$ (cm^3/mol)	$\Delta H°_{298}$ (kJ/mol)	$\Delta S°$ (J/K·mol)
$^1/_4Il + {}^3/_4Pv \rightarrow Ca_{0.25}Fe_{0.75}TiO_3$	−0.85	11.5	4.34
$^2/_3Ca_{0.25}Fe_{0.75}TiO_3 + {}^1/_3Pv \rightarrow Ca_{0.5}Fe_{0.5}TiO_3$	−0.003	5.03	2.53
$^1/_2Il + {}^1/_2Pv \rightarrow Ca_{0.5}Fe_{0.5}TiO_3$	−0.56	12.7	5.42
$^1/_2Ca_{0.5}Fe_{0.5}TiO_3 + {}^1/_2Il \rightarrow Ca_{0.25}Fe_{0.75}TiO_3$	−0.57	5.2	1.63

[a] Il = $FeTiO_3$ (ilmenite); Pv = $CaTiO_3$ (perovskite).

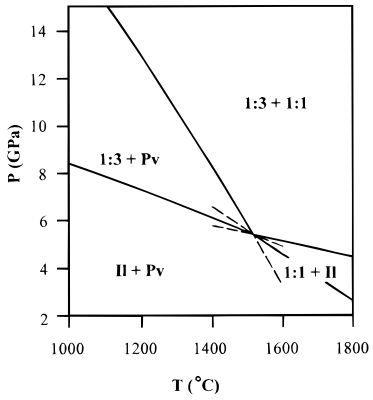

Figure 13. Phase relations at $FeCaTi_2O_6$ composition (Fe/(Fe + Ca) = 0.5) as a function of pressure and temperature.[58]

New B-site ordered perovskites have also been found in high-pressure experiments. The system $CaSiO_3$–$CaTiO_3$ at 9 GPa and 1200 °C shows a quenchable perovskite solid solution form $CaTiO_3$ to $CaTiO_{0.65}$-$Si_{0.35}O_3$, with the orthorhombic distortion decreasing to pseudocubic with increasing Si substitution.[10,59] At the $CaTi_{0.5}Si_{0.5}O_3$ composition, a sample quenched from 14 GPa and 1200 °C showed an ordered double perovskite structure with space group *Fm*3*m* and an alternation of Si-rich and Ti-rich octahedral sites along three axes.[10] Examination of this sample by HRTEM suggested the presence of lesser amounts of at least three other ordered perovskites.[10] Though some of these may be nonequilibrium features, the data suggest that high pressure favors ordered structures and that there may be a wealth of both A- and B-site ordered perovskites still to be discovered when pressure, temperature, and composition can each be varied systematically. Such ordered high-pressure perovskites may provide valuable comparisons to those formed at atmospheric pressure and studied for their applications as ferroelectrics, actuators, ion and proton conductors, and magnetic materials. High-pressure studies may well extend our understanding of the driving forces and mechanisms of ordering.

Conclusions

High-pressure reactions favor perovskite compounds in ABO_3 oxides. The lithium niobate structure can form as a quench phase for a restricted range of tolerance factors and ionic radii. The perovskites are generally high entropy phases and their formation reactions have

negative $P-T$ slopes. Transitions from ilmenite to perovskite are predicted for $CoTiO_3$ and $NiTiO_3$, with metastable quench products with lithium niobate structure likely. Such quench products are much less likely for silicates. The complete Fe−Mg substitution in titanate perovskites suggests there is no inherent instability to Fe^{2+} occupancy of the A site in the perovskite structure. The limited extent of the Fe−Mg substitution in silicate perovskites probably reflects a stabilization of the (Fe,Mg)O plus SiO_2 (stishovite) assemblage rather than any inherent instability for A-site divalent iron.

Ordered A-site perovskites in $CaTiO_3-FeTiO_3$ have high entropies and are favored both by high pressure and high temperature. A-site ordered perovskites containing other transition metals should be sought. The ability, through ordering and distortional transitions, to change the effective coordination of the A-site cation from 8 to 6 to 4 offers a richness of possible phases. In this context, the behavior of systems containing zinc and copper may be particularly interesting as these ions prefer tetrahedral and square planar coordination, respectively. It is anticipated that many other ordered perovskites will be found at high pressure and temperature.

Acknowledgment. Much of the work summarized here has been supported by a series of NSF solid state chemistry grants to A.N. and by CHiPR, the Center for High Pressure Research, and NSF Science and Technology Center. I thank K. D. Grevel, J. Majzlan, and C. Moss for help in manuscript and figure preparation.

References

(1) Navrotsky, A. *Physics and Chemistry of Earth Materials*; Cambridge University Press: Cambridge, U.K., 1994.
(2) Jeanloz, R.; Thompson, A. B. *Rev. Geophys. Space Phys.* **1983**, *21*, 51.
(3) Carmichael, I. S. E.; Turner, F. J.; Verhoogen, J. *Igneous Petrology*; McGraw-Hill: New York, 1974.
(4) Mehta, A.; Navrotsky, A. *A. J. Solid State Chem.* **1993**, *102*, 213.
(5) Newnham, R. E. *Perovskite, A Structure of Great Interest to Geophysics and Materials Science*; Navrotsky, A., Weidner, D., Eds.; American Geophysical Union: Washington, DC, 1989; p 91.
(6) Navrotsky, A. *Am. Mineral.* **1994**, *79*, 589.
(7) Brown, N. E.; Navrotsky, A.; Nord, G. L., Jr.; Banerjee, S. K. *Am. Mineral.* **1993**, *78*, 941.
(8) Glazer, M. A. *Acta Crystallogr.* **1972**, *B28*, 3384.
(9) Takayama-Muromachi, E.; Navrotsky, A. *J. Solid State Chem.* **1988**, *72*, 244.
(10) Leinenweber, K.; Grzechnik, A.; Voorhees, M.; Navrotsky, A.; Yao, N.; McMillan, P. F. *Phys. Chem. Miner.* **1997**, *24*, 528.
(11) Rossetti, G. H., Jr.; Rodriguez, M. A.; Navrotsky, A.; Cross, L. E.; Newnham, R. E. *Jour. Appl. Phys.* **1995**, *77*, 1683.
(12) Liu, X.; Wang, Y.; Liebermann, R. C.; Maniar, P. D.; Navrotsky, A. *Phys. Chem. Miner.* **1991**, *18*, 224.
(13) Navrotsky, A. *Prog. Solid State Chem.* **1987**, *17*, 53.
(14) Gillet, P.; Guyot, F.; Price, G. D.; Tournerie, B.; LeCleach, A. *Phys. Chem. Miner.* **1993**, *20*, 159.
(15) Ross, N. L.; Akaogi, M.; Navrotsky, A.; Susaki, J.; McMillan, P. F. *J. Geophys. Res.* **1986**, *91*, 4685.
(16) Fei, Y.; Saxena, S. K.; Navrotsky, A. *J. Geophys. Res.* **1990**, *95*, 6913.
(17) Anderson, O. L. *Am. Mineral.* **1998**, *83*, 23.
(18) Lu, R.; Hofmeister, A. M.; Wang, Y. *J. Geophys. Res.* **1994**, *99*, 795.
(19) Winkler, B.; Dove, M. T. *Phys. Chem. Miner.* **1992**, *18*, 407.
(20) Choudhury, N.; Chapelet, S. L.; Rao, K. R.; Ohise, S. *Pramana J. Phys.* **1988**, *30*, 423.
(21) Wentzkovich, R. M.; Ross, N. L.; Price, G. D. *Earth Planet. Sci. Interiors* **1995**, *90*, 101.
(22) Cohen, R. E.; Krakauer, H. *Ferroelectrics* **1992**, *136*, 65.
(23) Cohen, R. E.; Krakauer, H. *Phys. Rev.* **1990**, *B42*, 6416.
(24) Matsui, M. *Phys. Chem. Miner.* **1988**, *16*, 234.
(25) Stixrude, L.; Cohen, R. E. *Nature* **1993**, *364*, 613.
(26) Wang, Y.; Weidner, D. J.; Liebermann, R. C.; Liu, X.; Ko, J.; Vaughn, M. T.; Zhao, A.; Yaganeh-Haeri, A.; Pacalo, R. E. G. *Science* **1991**, *251*, 410.
(27) Wang, Y.; Guyot, F.; Liebermann, R. C. *Science* **1990**, *248*, 468.
(28) Funamori, H.; Yagi, T. *Geophys. Res. Lett.* **1993**, *20*, 387.
(29) Kanzaki, M.; Stebbins, J. F.; Xue, X. *Geophys. Res. Lett.* **1991**, *18*, 463.
(30) Mao, H. K.; Chen, L.-C.; Hemley, R. L.; Jephcoat, A. P.; Yu, Y. *J. Geophys. Res.* **1989**, *94*, 17889.
(31) Tamai, H.; Yagi, T. *Phys. Earth Planet. Interiors* **1989**, *54*, 370.
(32) Sherman, D. M. *J. Geophys. Res.* **1993**, *98*, 19795.
(33) Chizmeshya, A. V. G.; Wolf, G. H.; McMillan, P. F. *Geophys. Res. Lett.* **1996**, *23*, 2725.
(34) Akaogi, M. *J. Phys. Earth* **1995**, *43*, 457.
(35) Fei, Y.; Wang, Y.; Finger, L. W. *J. Geophys. Res.* **1996**, *101*, 11525.
(36) Akaogi, M.; Kojitani, H.; Matsuzaka, K.; Suzuki, T.; Ito, E. *High P−T Research, Properties of Materials;* Sueno, S.; Marghnani, M., Eds.; Terra Pub., in press.
(37) Topor, L.; Navrotsky, A., in preparation.
(38) Akaogi, M.; Ito, E. *Geophys. Res. Lett.* **1993**, *20*, 1839.
(39) Ashida, T.; Kume, S.; Ito, E.; Navrotsky, A. *Phys. Chem. Miner.* **1988**, *16*, 239.
(40) Yusa, H.; Akaogi, M.; Ito, E. *J. Geophys. Res.* **1993**, *98*, 6453.
(41) Liebertz, J.; Rooymans, C. J. M. *Z. Phys. Chem.* **1965**, *44*, 242.
(42) Morgenstern-Baderau, I., Poix, P.; Michel, M. *C. R. Acad. Sci. Paris* **1964**, *258*, 3036.
(43) Syono, Y.; Akimoto, S.; Ishikawa, Y.; Endoh, Y. *J. Phys. Chem. Solids* **1969**, *30*, 1665.
(44) Ito, E.; Matsui, Y. *Phys. Chem. Miner.* **1979**, *4*, 265.
(45) Ko, J.; Prewitt, C. T. *Phys. Chem. Miner.* **1988**, *15*, 355.
(46) Ross, N. L.; Ko, J.; Prewitt, C. T. *Phys. Chem. Miner.* **1989**, *16*, 621.
(47) Mehta, A.; Leinenweber, K.; Navrotsky, A. *Phys. Chem. Miner.* **1994**, *21*, 207.
(48) Leinenweber, K.; Utsumi, W.; Tsuchida, Y.; Yagi, T.; Kurita, K. *Phys. Chem. Miner.* **1991**, *18*, 244.
(49) Linton, J. A.; Fei, Y.; Navrotsky, A. *Am. Mineral.* **1997**, *82*, 639.
(50) Linton, J. A.; Fei, Y.; Navrotsky, A. *Am. Mineral.* **1998**, (in press).
(51) Ko, J.; Brown, N. E.; Navrotsky, A.; Prewitt, C. T.; Gasparik, T. *Phys. Chem. Miner.* **1989**, *16*, 727.
(52) Neil, J. M.; Navrotsky, A.; Kleppa, O. J. *Inorg. Chem.* **1971** *10*, 2076.
(53) McCammon, C. A. *Phys. Chem. Miner.* **1998**, *25*, 292.
(54) Kimura, S.; Muan, A. *Am. Mineral.* **1971**, *56*, 1333 and 1347.
(55) Leinenweber, K.; Parise, J. B. *J. Solid State Chem.* **1995**, *114*, 277.
(56) Leinenweber, K.; Linton, J. A.; Navrotsky, A.; Fei, Y.; Parise, J. B. *Phys. Chem. Miner.* **1995**, *22*, 251.
(57) Yao, N.; Navrotsky, A.; Leinenweber, K. *J. Solid State Chem.* **1996**, *123*, 73.
(58) Linton, J. A.; Navrotsky, A.; Fei, Y. *Am. Mineral.* **1998** (in press).
(59) Kubo, A.; Suzuki, T.; Akaogi, M. *Phys. Chem. Miner.* **1997**, *24*, 488.
(60) Ito, Y.; Matsui, M. *Phys. Chem. Miner.* **1970**, *4*, 265.
(61) Akaogi, M.; Navrotsky, A. *Phys. Chem. Miner.* **1987**, *14*, 435.
(62) Akaogi, M.; Navrotsky, A. *Phys. Chem. Miner.* **1985**, *12*, 317.
(63) Leinenweber, K.; McMillan, P. F.; Navrotsky, A. *Phys. Chem. Miner.* **1989**, *16*, 799.
(64) Ross, N. L.; Navrotsky, A. *Am. Mineral.* **1988**, *73*, 1355.
(65) Akaogi, M.; Yusa, H.; Ito, E.; Yagi, T.; Suito, K.; Iiyama, J. T. *Phys. Chem. Miner.* **1990**, *17*, 17.
(66) Gasparik, T.; Wolf, K.; Smith, C. M. *Am. Mineral.* **1994**, *79*, 1219.
(67) Grzechnik, A.; Hubert, H.; McMillan, P. F.; Petuskey, W. *Integr. Ferroelectrics* **1997**, *15*, 191.
(68) Syono, Y.; Akimoto, S.; Endoh, Y. *J. Phys. Chem. Solids* **1971**, *32*, 243.
(69) Ito, E. *Materials Science of the Earth's Interior*; Sunagawa, I., Ed.; Terra Scientific: Tokyo, Japan, 1984; pp 387−94.

CM9801901